Conductance fluctuations in graphene systems: The relevance of classical dynamics

Lei Ying,[1] Liang Huang,[1,2] Ying-Cheng Lai,[1,3,4] and Celso Grebogi[4]
[1]*School of Electrical, Computer, and Energy Engineering, Arizona State University, Tempe, Arizona 85287, USA*
[2]*Institute of Computational Physics and Complex Systems, and Key Laboratory for Magnetism and Magnetic Materials of MOE, Lanzhou University, Lanzhou, Gansu 730000, China*
[3]*Department of Physics, Arizona State University, Tempe, Arizona 85287, USA*
[4]*Institute for Complex Systems and Mathematical Biology, King's College, University of Aberdeen, Aberdeen AB24 3UE, United Kingdom*
(Received 23 April 2012; revised manuscript received 15 June 2012; published 28 June 2012)

Conductance fluctuations associated with transport through quantum-dot systems are currently understood to depend on the nature of the corresponding classical dynamics, i.e., integrable or chaotic. However, we find that in graphene quantum-dot systems, when a magnetic field is present, signatures of classical dynamics can disappear and universal scaling behaviors emerge. In particular, as the Fermi energy or the magnetic flux is varied, both regular oscillations and random fluctuations in the conductance can occur, with alternating transitions between the two. By carrying out a detailed analysis of two types of integrable (hexagonal and square) and one type of chaotic (stadium) graphene dot system, we uncover a universal scaling law among the critical Fermi energy, the critical magnetic flux, and the dot size. We develop a physical theory based on the emergence of edge states and the evolution of Landau levels (as in quantum Hall effect) to understand these experimentally testable behaviors.

DOI: 10.1103/PhysRevB.85.245448 PACS number(s): 72.80.Vp, 05.45.Mt, 73.23.−b, 73.63.−b

I. INTRODUCTION

A fundamental problem in quantum transport through nanoscale devices is conductance fluctuations. Consider, for example, a quantum-dot system. As the Fermi energy of the conducting electrons is varied, the conductance can exhibit fluctuations of distinct characteristics, depending on the geometrical shape of the dot. Research in the past two decades has demonstrated that the nature of the corresponding classical dynamics can play a key role in the conductance-fluctuation pattern.[1–4] For example, when the classical scattering dynamics is integrable or has a mixed phase-space structure, there can be sharp resonances in the conductance curve. However, when the classical dynamics is fully chaotic, the conductance variations tend to be smoother.

There have been tremendous recent efforts in graphene[5–8] due to its relativistic quantum physical properties and its potential for applications in nanoscale electronic devices and circuits. The study of transport in open graphene devices is thus a problem of vast interest.[8] For example, the role played by disorder in conductance fluctuations in graphene was investigated, where anomalously strong fluctuations[9] or suppression of the fluctuations[10] were reported. A recent work has revealed that, in graphene quantum dots, the characteristics of conductance fluctuations also depend on the nature of the classical dynamics similar to those for conventional two-dimensional electron-gas (2DEG) quantum-dot systems.[11] In these recent works, magnetic field is absent. The magnetic properties of graphene, however, are different from those associated with 2DEG systems. For example, in graphene the quantum Hall effect can be observed even at room temperature due to the massless Dirac fermion nature of the quasiparticles and significantly reduced scattering effects.[12] Especially, the linear energy-momentum relation[13] in graphene stipulates that the Landau levels are distributed according to $\pm\sqrt{N}$, where N is the Landau index, as opposed to the proportional dependence on N in 2DEG systems.[14]

In this paper, we study conductance fluctuations in graphene quantum-dot systems in the presence of magnetic field. We present two main results. First, in the parameter plane spanned by the perpendicular magnetic flux and the Fermi energy, there are regions of regular and random conductance oscillations, respectively. As the Fermi energy or the magnetic flux is changed, the fluctuations can be either regular or random, implying a kind of "coexistence" of regular and irregular conductance fluctuations as a single physical parameter is varied. Second, an experimentally significant issue is how conductance fluctuations are affected by the size of the quantum dot in the presence of a perpendicular magnetic field. In a previous experimental study[15] of quantum dots of sizes ranging from 0.7 to 1.2 μm, the authors found nearly periodic conductance oscillations as the magnetic-field strength is varied. The frequency of the oscillation pattern, the so-called magnetic frequency, was found to follow a scaling relation with the edge size of the dot.[15] In a recent study of the magnetic scaling behavior in graphene quantum dots,[16,17] it was found that for small dots of edge size less than 0.3 μm, the magnetic frequency exhibits a scaling relation with the dot area. Here we shall focus on an important set of scarred orbits and examine the resulting conductance oscillations. We find that, for graphene quantum dots, below the first Landau level, the conductance exhibits periodic oscillations with the magnetic flux and with the Fermi energy. In fact, the magnetic frequency scales linearly with the dot size. However, the energy frequency, the inverse of the variation in the Fermi energy for the conductance to complete one cycle of oscillation, scales inversely with the dot size. Beyond the regime of periodic conductance oscillations, new sets of scarred orbits emerge and evolve as successive Landau levels are crossed, each with its own period, leading to random conductance fluctuations. The remarkable feature is that these scaling behaviors are independent of the nature of the underlying classical dynamics, i.e., regular or chaotic. Considering that a large body of existing literature points to the critical role played by the nature of the classical dynamics in conductance fluctuations,[1–4] our finding that the presence of magnetic field can greatly suppress this sensitivity to classical dynamics is striking.

The rest of the paper is organized as follows. Section II describes briefly the tight-binding Hamiltonian and the nonequilibrium Green's function method to calculate the conductance for graphene quantum dots. Extensive evidence of periodic conductance oscillations and the emergence of random conductance fluctuations is presented in Sec. III. In Sec. IV, we develop a theoretical understanding of the numerical results based on the emergence of edge states and semiclassical quantization. Conclusive remarks are presented in Sec. V.

II. GRAPHENE QUANTUM DOTS AND CONDUCTANCE CALCULATION

We use the standard tight-binding framework[18] to compute the conductances through graphene quantum dots of various geometrical shapes, where p_z orbitals and nearest-neighbor hopping are assumed. The tight-binding Hamiltonian has the form

$$H = \sum_{i,j} -t_{ij}(c_i^\dagger c_j + \text{H.c.}), \tag{1}$$

where the summation is over all nearest-neighbor pairs and $c_i^\dagger$ (c_j) is the creation (annihilation) operator, t_{ij} is the hopping energy[7] from atom j and to atom i, and the onsite energy has been set as the reference energy as it is the same for all the atoms. In the absence of magnetic field, the nearest-neighbor hopping energy is $t_{ij} = t_0 = 2.7\,\text{eV}$. When a perpendicular uniform magnetic field $\mathbf{B}$ with vector potential $\mathbf{A} = (-By,0,0)$ is applied, the hopping energy is altered by a phase factor:

$$t_{ij} = t_0 \exp(-i2\pi\phi_{i,j}), \tag{2}$$

where $\phi_{i,j} = (1/\phi_0)\int_j^i \mathbf{A}\cdot d\mathbf{l}$, and $\phi_0 = h/e = 4.136 \times 10^{-15}\,\text{Tm}^2$ is the magnetic flux quanta. For convenience, we use magnetic flux through a hexagonal plaque of graphene, $\phi = BS$, as a control parameter characterizing variations in the magnetic-field strength, where S is the area of the hexagonal plaque composed of six carbon atoms. Thus, $S_0 = 3\sqrt{3}a_0^2/2$, where $a_0 = 1.42$ Å. Here, we treat graphene devices as flat two-dimensional systems. Large ripples modify the hopping and can induce localization and additional transport fluctuations.[19]

At low temperature, the conductance G of a quantum-dot device is approximately proportional to transmission T and is given by the Landauer formula:[20] $G(E) = (2e^2/h)T_G(E)$. The standard nonequilibrium Green's function (NEGF) method[21,22] can be used to calculate the transmission, which can be expressed by[18,23]

$$T(E) = \text{Tr}(\Gamma_L G_D \Gamma_R G_D^\dagger), \tag{3}$$

where G_D is the Green's function of the device given by $G_D = (EI - H_D - \Sigma_L - \Sigma_R)^{-1}$, H_D is the Hamiltonian of the closed device, the semi-infinite leads are accounted for by the self-energies Σ_L and Σ_R, and $\Gamma_{L,R}$ are the coupling matrices given by

$$\Gamma_{L,R} = i(\Sigma_{L,R} - \Sigma_{L,R}^\dagger). \tag{4}$$

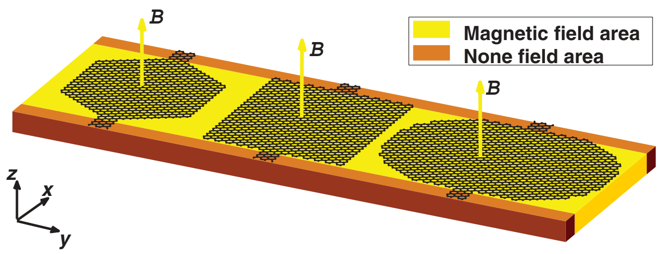

FIG. 1. (Color online) Schematic illustration of hexagonal-, square-, and stadium-shaped graphene quantum dots in a perpendicular magnetic field. Note that the magnetic field exists only in the device region.

The local density of states (LDS) for the device is

$$\rho = -\frac{1}{\pi}\text{Im}[\text{diag}(G_D)]. \tag{5}$$

To be representative, we consider graphene quantum dots of three different geometric shapes: hexagonal, square, and stadium, as shown in Fig. 1. Hexagonal geometry is interesting due to the graphene lattice symmetry, i.e., the boundaries consist of zigzag edges only. Thus, regardless of the device size, the boundaries remain to be zigzag. The square geometry has both zigzag and armchair boundaries along the two perpendicular directions, respectively. The classical dynamics in these two structures are integrable. The stadium-shaped quantum dot, however, has chaotic dynamics in the classical limit, which has been used as a paradigmatic system in the quantum-chaos literature to explore various quantum manifestations of classical chaos.[24]

The geometrical parameters of the three types of devices are as follows. For the hexagonal geometry the height (the distance between the two parallel boundaries) is 10.934 nm. The width of the lead is 1.136 nm, which is chosen somewhat arbitrarily. For the square device the width is 10.934 nm and the width of the lead is 1.136 nm so that the overall size is comparable to the hexagonal dot. The size of the rectangular part of the stadium dot structure is 16.898 ×10.988 nm and its lead width is 1.136 nm.

III. NEARLY PERIODIC CONDUCTANCE OSCILLATIONS AND EMERGENCE OF RANDOM CONDUCTANCE FLUCTUATIONS

Figures 2–4 are representative examples of conductance variations either with the Fermi energy for fixed magnetic flux or with the magnetic flux for fixed Fermi energy, for the hexagonal, square, and stadium dot shape, respectively. In all cases, a critical point can be identified unequivocally (denoted by either E_1 or ϕ_1), where the conductance variations are nearly periodic on one side of the point and random on the other side. In particular, for all three geometrical shapes, for fixed magnetic flux, the conductance varies quite regularly for $E < E_1$ but randomly for $E > E_1$. For fixed Fermi energy, the conductance variations are regular for $\phi > \phi_1$ and random for $\phi < \phi_1$. Better insights into the transition from regular to random conductance variations (or vice versa) can be gained by examining the typical LDS patterns about the critical point. For example, for the hexagonal geometry, there is a circularly localized pattern at $E_1 = 0.2350t$, as shown

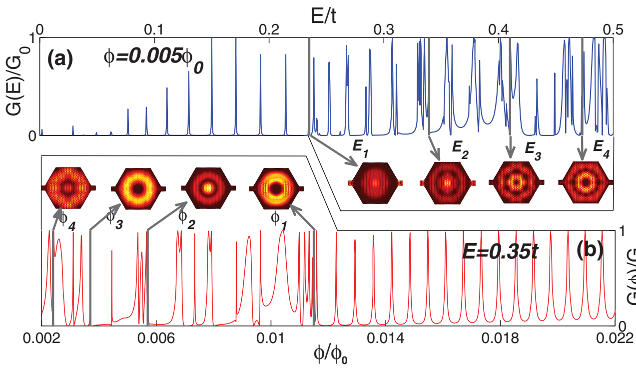

FIG. 2. (Color online) Conductances of the hexagonal-shaped quantum dot. The height of the dot is $W_D = 10.934$ nm and the lead width is $W_L = 1.136$ nm. The device region contains 4158 carbon atoms. (a) Conductance versus the Fermi energy E_F for fixed magnetic field $\phi = 0.005\phi_0$. The energy values of the shown LDS patterns are those of the Landau levels: $E_1 = 0.2350t$, $E_2 = 0.3395t$, $E_3 = 0.4100t$, and $E_4 = 0.4730$t, respectively. (b) Conductance versus the magnetic flux ϕ for fixed Fermi energy $E = 0.35t$. At this energy, there are Landau levels located at $\phi_1 = 0.0115\phi_0$, $\phi_2 = 0.0057\phi_0$, $\phi_3 = 0.0037\phi_0$, and $\phi_4 = 0.0024\phi_0$ (from large to small). The corresponding LDS patterns are also shown.

in Fig. 2(a), where the conductance of the dot structure is effectively zero due to the localization of conducting electrons inside the device. Figure 2(a) also displays several similar, recurring LDS patterns at E_2, E_3, and E_4. The ratios among these energy values are $E_1 : E_2 : E_3 : E_4 = 1 : 1.44 : 1.74 : 2.01 \approx 1 : \sqrt{2} : \sqrt{3} : 2$. We observe that the energy values are approximately proportional to $\sqrt{N}$, where N is the index of E_N. These behaviors have also been observed for the square and stadium-shaped quantum dots. For example, Fig. 3(a) shows, for the square geometry, occurrences of the transition between regular and random conductance fluctuations at $E_1 : E_2 : E_3 = 0.2344t : 0.3289t : 0.4021t \approx 1 : \sqrt{2} : \sqrt{3} : 2$ for fixed magnetic flux $0.005\phi_0$. The ratio is also consistent with the Landau level distribution as in Eq. (6) below. In Fig. 3(b), the Fermi energy is fixed at $E = 0.4t$, and the transition points are $\phi_1 : \phi_2 : \phi_3 = 0.01508\phi_0 : 0.00756\phi_0 : 0.00501\phi_0 = 1 : 1/1.99 : 1/3.00$, which are consistent with Eq. (7) (to be discussed below). For the stadium-shaped device, the conductance curve shares the same features as Figs. 2 and 3. The transition points (as indicated in the figure and the caption) also fit into the same Landau level distribution as given by Eqs. (6) and (7) below. These numerical results indicate that the coexistence of regular and random conductance fluctuations and the transitions between them are determined by the Landau levels, regardless of the geometric shape of the graphene quantum dot. Note that, however, the LDS patterns do depend on the geometrical shape of the dot.

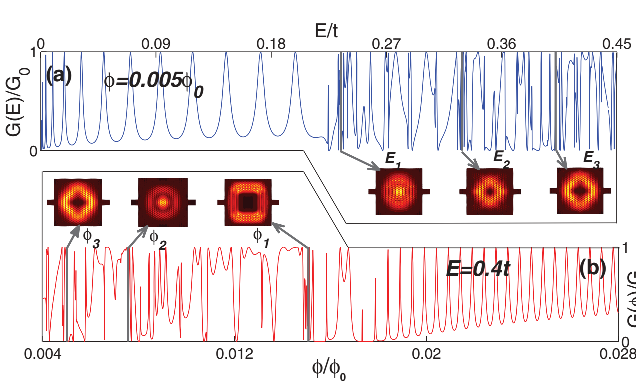

FIG. 3. (Color online) Conductance variations in a square graphene quantum dot of side length $W_D = 10.934$ nm and lead width $W_L = 1.136$ nm, which contains 4802 atoms. (a) For fixed magnetic flux, Landau levels are located at $E_1 = 0.2344t$, $E_2 = 0.3289t$, and $E_3 = 0.4021t$, and so on. In (b) where the Fermi level is fixed, the transition points are $\phi = 0.01508\phi_0$, $0.00756\phi_0$, $0.00501\phi_0$, and so on.

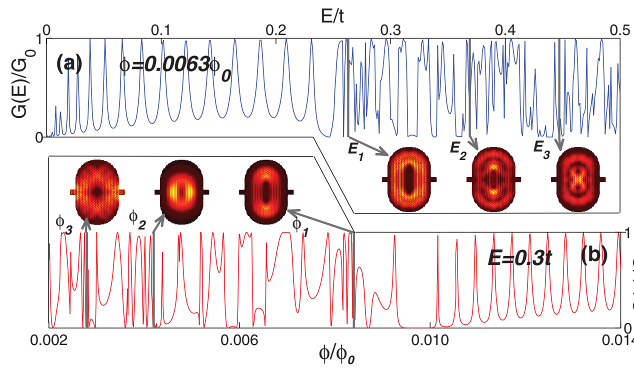

FIG. 4. (Color online) Conductance variations in the stadium geometry. The rectangular region of this chaotic dot has the dimensions $W_D = 16.898$ nm and 10.988 nm, and the lead size is $W_L = 1.136$ nm. The stadium shape contains 6410 atoms. Energy Landau levels are located at $E_1 = 0.263t$, $E_2 = 0.369t$, and $E_3 = 0.4471t$, and so on for fixed magnetic flux. For fixed Fermi energy $E = 0.3t$, the magnetic Landau levels occur at $\phi = 0.0084\phi_0$, $0.0042\phi_0$, $0.0028\phi_0$, and so on.

In nonrelativistic quantum, 2DEG systems of infinite size, the Landau levels are distributed linearly with the level index N as $E_N = (N + 1/2)(eB\hbar/m)$. However, for relativistic quantum quasiparticles in graphene, due to the linear energy-momentum relation $E = v_F k$ near the Dirac point, the Landau levels are distributed according to[25]

$$E(N) = \pm\omega_c\sqrt{N}, \tag{6}$$

where $\omega_c = \sqrt{2}v_F/\ell_B$ is the cyclotron frequency of Dirac fermions (electrons) and $\ell_B = \sqrt{\hbar/eB}$ is the magnetic length. When a Landau level rises, the charge carriers are localized approximately at the center of the device, leading to a near-zero conductance. The numerically obtained LDS patterns thus indicate that the critical energy values, for example, in Fig. 2(a), are nothing but the Landau levels.

From Eq. (6), we can obtain the corresponding Landau levels in terms of the magnetic flux for fixed Fermi energy:

$$B(N) = \frac{\hbar E^2}{2ev_F^2}\frac{1}{N}. \tag{7}$$

This formula can be verified by noting that, for example, as shown in Fig. 2(b), for fixed Fermi energy at $E = 0.35t$ in the hexagonal dot, varying the magnetic field also partitions the conductance curve into different regions with regular and random conductance fluctuations. The critical magnetic fluxes are $\phi_1 = 0.0115\phi_0$, $\phi_2 = 0.0057\phi_0$, $\phi_3 = 0.0037\phi_0$, and

$\phi_4 = 0.0024\phi_0$, leading to the approximate ratios of $1 : 1/2 : 1/3 : 1/4$, which is consistent with Eq. (7).

IV. SEMICLASSICAL THEORY OF REGULAR CONDUCTANCE OSCILLATIONS AND UNIVERSAL TRANSITION TO RANDOM CONDUCTANCE FLUCTUATIONS

Our numerical computations indicate strongly that the emergence and properties of the Landau levels are key to understanding the origin of regular conductance oscillations in the presence of magnetic field. In fact, significant physical insights can be gained from the phenomenon of integer quantum Hall effect in semiconductor 2DEG systems, which is a direct manifestation of the evolution of the Landau levels. In that case, when the magnetic field strength is fixed and the Fermi energy is increased, the conductance reaches minimum when the Fermi energy is at a Landau level and takes on a much larger value when the Fermi energy is in between two neighboring Landau levels. This is contrary to the behavior of the density of the states, which is appreciable only at the Landau levels. The basic reason is that, for a quantum dot, at the Landau level the charge carriers tend to be localized in the central region of the dot and so cannot participate in the transport process. However, when the Fermi energy is in between two adjacent Landau levels, *edge states* arise which circulate around the boundary of the quantum dot, facilitating a strong coupling with the propagating modes in the semi-infinite leads and resulting in a large conductance. In our case, there is a new feature. Between two neighboring Landau levels, the energy difference ΔE_h, where the subscript "h" stands for Hall effect, is enormous so that, besides the formation of the circular edge states associated with the quantum Hall effect, another class of circular edge states can be formed, as stipulated by the semiclassical Bohr-Sommerfield quantization condition. This introduces another energy period ΔE_q, where "q" stands for quantization, in which the Bohr-Sommerfield edge states form and disappear. Since the circular edge states facilitate transport through the quantum dot and since ΔE_q is typically smaller than ΔE_h, the fulfillment of the semiclassical quantization condition contributes to *fine-scale* oscillations in the conductance curve.

To exploit the Bohr-Sommerfield quantization condition for the edge states in graphene, it is convenient to modify the size of the device but keep the geometric shape unchanged. Without loss of generality, we focus on the hexagonal geometry that possesses zigzag boundaries. We choose (somewhat arbitrarily) several heights of the hexagonal devices: $W_{D1} = 19.454$ nm, $W_{D2} = 10.934$ nm, and $W_{D3} = 6.674$ nm with the relative ratio $W_{D1} : W_{D2} : W_{D3} = 2.9 : 1.7 : 1$. Figure 5 shows, for these devices, periodic conductance oscillations below the first Landau level.

Bohr-Sommerfield quantization theory stipulates that the action integral for two successive edge states satisfies the condition[26] $\Delta I = h$, where h is the Planck constant and $I = \oint \mathbf{p} \cdot d\mathbf{q}$. In the presence of a magnetic field with vector potential $\mathbf{A}$, the generalized momentum is $\mathbf{p} = \hbar\mathbf{k} + e\mathbf{A}$ and the wave vector $\mathbf{k}$ has the same direction as $d\mathbf{q}$. For a given periodic orbit of length L, we have

$$I = |\mathbf{p}|L = \hbar|\mathbf{k}|L + eBS, \tag{8}$$

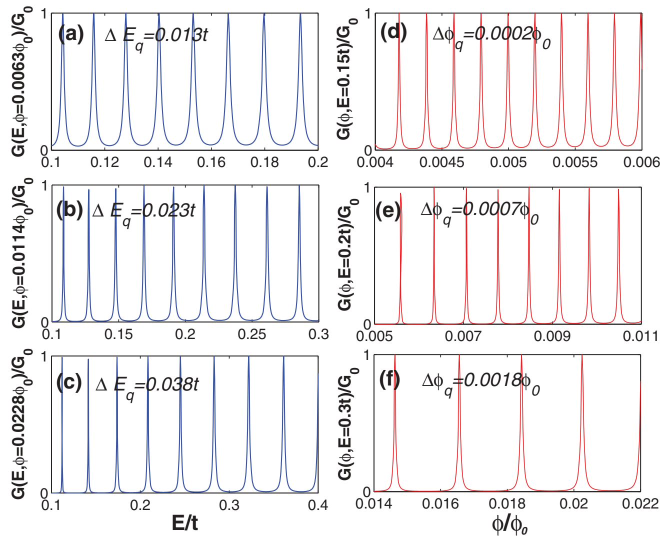

FIG. 5. (Color online) Conductance oscillations in hexagonal quantum dots of different sizes. The device width for (a) and (d) is $W_D = 19.454$ nm and it contains 12938 atoms, for (b) and (e) it is $W_D = 10.934$ nm and the device has 4158 atoms. In (c) and (f), the device has width $W_{D3} = 6.674$ nm and 1616 atoms. Every subfigure indicates the period of the regular oscillations.

where S is the area that the periodic orbit encloses in the physical space. For a fixed magnetic-field strength, we then have $\Delta kL = 2\pi$, where L is length of the periodic orbit. For graphene, we have $E = \hbar v_F k$ near the Dirac point, so the relationship between the energy interval ΔE_q due to the quantization condition and the length of the periodic orbit is

$$\Delta E_q = hv_F/L. \tag{9}$$

Due to the different boundary conditions in two dimensions, we only test the ratio of the energy interval. In Figs. 5(a), 5(c), and 5(e), the energy intervals can be determined, giving the ratios $\Delta E_{q1} : \Delta E_{q2} : \Delta E_{q3} = 1/L_1 : 1/L_2 : 1/L_3 = 1 : 1.76 : 2.92$, which are quite close to the inverse ratios of the device size $1/W_{D1} : 1/W_{D2} : 1/W_{D3} = 1 : 1.7 : 2.9$. Moreover, for $L = W_D$, we can estimate the Fermi velocity $v_F = \Delta E_q W_D/h \approx 10^6\ m/s$, which is close to the Fermi velocity calculated from the dispersion curve. This means that the length of the circulating orbit is comparable to the device height, indicating that the effective diameter of the orbit is smaller than that of the device. We thus see that the regular conductance oscillations are a consequence of the Bohr-Sommerfield quantization of the edge states between two Landau levels. In particular, when the quantization condition is satisfied, a strong LDS pattern emerges at the edge of the device, as shown in Fig. 6, which bridges with the transmitting modes in the two leads and leads to the peak value $2e^2/h$ for the conductance. On the contrary, when the quantization condition is violated, edge states cannot form, giving rise to minimal conductance. Similarly, for fixed Fermi energy, or equivalently, fixed wave-vector (from the dispersion relation), the quantization condition becomes $\Delta(eBS) = h$, or

$$\Delta\phi = \Delta BS = \phi_0, \tag{10}$$

where $\phi_0 = h/e$ is the magnetic flux quanta. Since the edge states typically circulate the device boundaries, S is

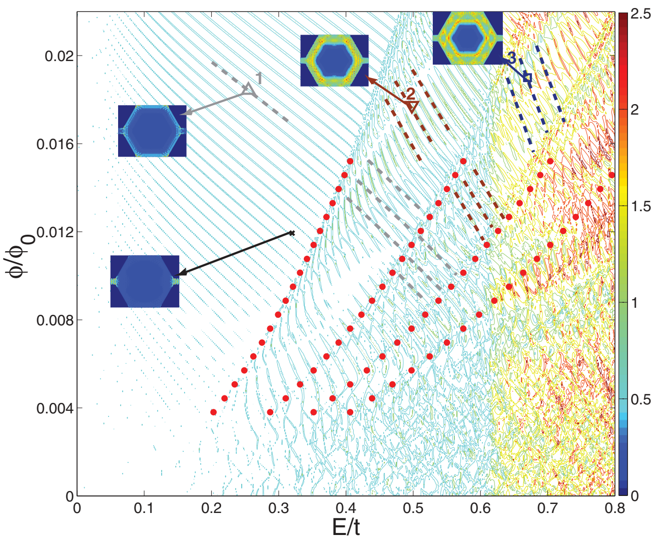

FIG. 6. (Color online) A hexagonal geometry device with 4158 atoms. Colors of the contour lines represent conductance G/G_0. The red dash lines are four Landau-levels, which divide the $G \sim E \sim \phi$ contour into several distinct regions. In each region, there are one or several conductance fluctuation patterns (patterns 1,2,3). Each conductance pattern corresponds a distinct LDS pattern.

proportional to the area of the device. From Figs. 5(b), 5(d), and 5(f), we obtain $\Delta\phi_{q1} : \Delta\phi_{q2} : \Delta\phi_{q3} = 1 : 3.2 : 9 \approx 1/W_{D1}^2 : 1/W_{D2}^2 : 1/W_{D3}^2$. Compared with the numerical results of ΔE_q, the error in $\Delta\phi_q$ is larger due to our approximation of S. When the area surrounded by the circulating orbit is determined more precisely, we find that the magnetic quantization condition [Eq. (10)] is satisfied. Note that in the absence of magnetic field or if the field is weak, edge states occur only at zigzag boundaries. However, under a strong magnetic field (above the first Landau level), edge states can emerge for both armchair and zigzag boundaries.

From the above analysis of the Bohr-Sommerfeld quantization condition, we find that the conductance oscillations are related to the Fermi energy, the magnetic-field strength, and the size of the device. To obtain a quantitative scaling relationship among those parameters, we develop the following physical analysis. Theoretically, the size of a device is related to the electron cyclotron radius at the Fermi energy, because only the electrons near the Fermi surface contribute to device transmission or conductance. The ratio of the cyclotron surrounding area and perimeter is given by[17]

$$S/L = k_F \ell_B^2, \tag{11}$$

where S/L can be regarded as a single parameter characterizing the device size. In a graphene system, the energy near a Dirac point is proportional to the Fermi wave-vector k_F: $E_F = \hbar v_F k_F$ or $k_F = E_F/(\hbar v_F)$, where the Fermi velocity is given by $v_F = \sqrt{3}t_0 a/2\hbar$ and $a = 2.46$ Å is the graphene lattice constant. Substituting these back into Eq. (11), we obtain the relationship of Fermi energy E, the device size D, and the magnetic flux ϕ as follows:

$$S/L = \frac{2\hbar S_0}{\sqrt{3}eat_0}\frac{E}{\phi}, \tag{12}$$

or in a different form as (for a given, fixed device size)

$$S/L = \frac{2\hbar S_0}{\sqrt{3}eat_0}\frac{\Delta E}{\Delta\phi}. \tag{13}$$

This relation can be used to infer the characteristic size D of the device from the conductance oscillations. For example, for the hexagonal geometry, $S = \sqrt{3}D^2/2$ and $L = 2\sqrt{3}D$. The scaling relation can be modified to

$$D_{\text{hex}} = \frac{12\hbar S_0}{\sqrt{3}eat_0}\frac{\Delta E}{\Delta\phi}, \tag{14}$$

which can be readily verified numerically. In particular, since the curves shown in Fig. 5 are for the edge states circulating the device, we can use ΔE and $\Delta\phi$ from the figure to infer the corresponding values of D, which yields $D_1 = 13.926$ nm, $D_2 = 7.836$ nm, and $D_3 = 4.734$ nm. Comparing with the actual size of the dot W_D as described in the caption of Fig. 5, we observe somewhat large discrepancies. However, if we compare the ratios, we have $D_1 : D_2 : D_3 = 2.94 : 1.655 : 1$, which are extremely close to the ratios of the actual dot sizes $W_{D1} : W_{D2} : W_{D3} = 2.915 : 1.640 : 1$. We also see that, for the three dot sizes, the ratio W_D/D is the same, which is about 1.4. The discrepancies in the actual size are caused by the approximation in Eq. (11) and by the assumption that the diameter of the circulating orbits is equal to the device size. Nevertheless, since the estimated values of D and W_D are of the same order of magnitude, it can be used to infer the dot size from the conductance oscillations versus the Fermi energy and the magnetic flux, which can be used as corroborative evidence and be compared with other direct/indirect measurements.

The scaling relation (14) may be feasibly observed experimentally in graphene quantum dots because, for low Fermi energy, the underlying phenomenon emerges even when the applied magnetic field is weak, i.e., $\phi \to 0$. For conventional semiconductor 2DEG systems with a parabolic energy-momentum relation, similar scaling can in principle be observed but only for enormous magnetic field, as we have verified numerically. In particular, for a graphene quantum dot of size $D \sim 1\,\mu$m, the minimally required magnetic-field strength to observe the periodic conductance oscillations is about $3T$. While for a 2DEG device of the same size as 1 μm made of GaAs/AlGaAs heterogeneous structure, the minimum magnetic field required is[27] about $10T$.

To obtain a global view of the conductance oscillations/fluctuations in terms of a combination of Eqs. (6) and (7), we overlay the Landau levels on top of the contour plot of the conductance versus both energy E and magnetic flux ϕ for the hexagonal dot, as shown in Fig. 6. We see that the Landau levels divide the whole parameter space of (E, ϕ) into different regions with behaviors ranging from regular, parallel line patterns to complicated irregular patterns.[28] We have analyzed the case that the Fermi energy is below the first Landau level, where the edge states recur with the period ΔE_q, leading to regular conductance oscillations of the same energy period. For $E_F > E_1$, there are two sets of edge states, leading to two uncorrelated repetitive patterns, each with its own period ΔE_q. This is also manifested in Fig. 6 for the hexagonal dot that, in region 2 (between the first and the second Landau levels), there are two sets of conductance lines: one with the same slope as in region 1 (the overlapped gray lines) and another with a larger slope (brown lines) that originates in this region but persists in regions between higher Landau levels. In region 3 a new pattern appears, as indicated by the blue dashed lines in Fig. 6. The corresponding edge states are also shown in Fig. 6 for these typical line segments. We see that, for a fixed magnetic flux, as the Fermi energy is increased across a Landau level, a new set of edge states appears, adding a new set of line segments in the conductance plot. Since the energy period ΔE_q is uncorrelated for different types of edge states, as can be seen from Fig. 6, the conductance will fluctuate randomly when there are many sets of edge states. This explains the transition from regular conductance oscillations to random conductance fluctuations, as shown in Figs. 2(a), 3(a), and 4(a). A similar analysis can be carried out when the magnetic flux is varied [Figs. 2(b), 3(b), and 4(b)]. Since the transition is caused by the crossing of Landau levels and the variation of the edge states, it holds regardless of the detailed geometric shape of the quantum dot and the nature of the underlying classical dynamics, i.e., integrable or chaotic. The transition can thus be characterized as universal.

While our discussion has been focused on the hexagonal dot, here we briefly show that the same mechanism leading to regular conductance oscillations and the transition to random fluctuations holds for other geometries as well. To demonstrate this in a comprehensive manner, we show in Fig. 7 the conductance in the (ϕ,E) plane for all three cases. We see

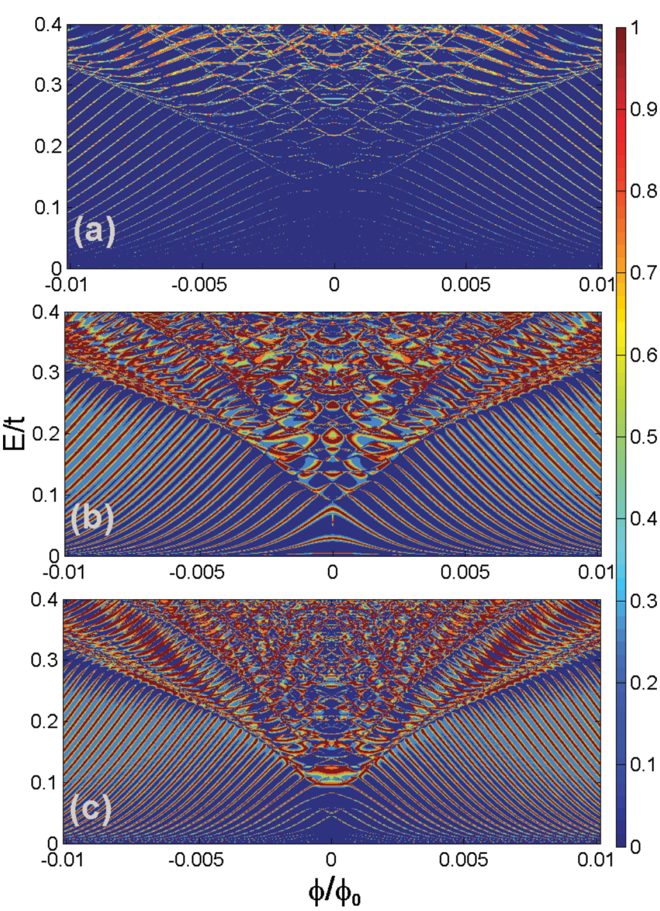

FIG. 7. (Color online) (a)–(c) Conductance $G(E,\phi)$ for the hexagonal-, square-, and stadium-shaped graphene quantum dots, respectively, where the colors indicate the values of the conductance.

that the conductance is symmetric with respect to reversal of the magnetic flux $[T(\phi) = T(-\phi)]$ due to the two-terminal characteristic of our device.[18] The patterns of the conductance oscillations and fluctuations for the three cases are apparently similar, due to the fact that the patterns are all partitioned by the Landau levels [e.g., Eq. (6)] that do not depend on the geometric details of the device. However, the fine structures can be different. First, below the first Landau level, the slopes of the line patterns indicate the size of the device because the edge states are exactly circulating the "edge" of the device (Fig. 6), which are slightly different for the three cases. Second, above the first Landau level, the details of the conductance patterns are more distinct. This is because, in contrast to the edge states below the first Landau level, these states are now more dispersive and also depend on the shape of the device (comparing the LDS patterns in Figs. 2–4). Third, conductance fluctuations in the chaotic stadium billiard tend to be more smooth as compared with those in the two integrable cases.[29,30] This feature is especially pronounced in the small-ϕ regime. When the classical dynamics is chaotic, the characteristic energy scale in the conductance-fluctuation pattern of the underlying quantum dot tends to be much larger,[11] leading to a smoother variation. For quantum dots with integrable or mixed dynamics, there are sharp resonances in the conductance-fluctuation curves. This can be seen, e.g., from the sudden change of the color scale from blue to red, or vice versa, in Fig. 7(b) for $\phi \sim 0$. [In the chaotic case, the change in the color scale is much more smooth, as shown in Fig. 7(c)]. In addition, in the chaotic graphene quantum dot, there is level repelling, which can also be seen from Fig. 7(c) in the $\phi \sim 0$ regime, where the conductance lines tend to avoid each other, a feature that is absent in both Figs. 7(a) and 7(b).

V. CONCLUSION

Previous works on conductance fluctuations associated with transport through nanoscale, quantum-dot systems emphasized the difference between situations where the underlying classical dynamics are chaotic or integrable.[1–4] A general understanding is that Fano-type[31] of sharp resonances typically occur in dot systems with integrable classical dynamics, and chaos can effectively smooth out these resonances quantum-mechanically. This picture holds for both 2DEG and graphene systems in which the quantum dynamics are nonrelativistic and can be relativistic, respectively, and it has been suggested recently[32] that altering classical chaos can effectively modulate quantum transport in terms of conductance-fluctuation patterns.

We find that the presence of magnetic field can alter the existing understanding of the quantum manifestations of classical chaos in that the difference in the quantum transport as caused by different types of classical dynamics can diminish. As a result, universal behaviors emerge. The remarkable phenomenon has been observed in graphene quantum dots of integrable and chaotic geometries. In particular, the conductance curves contain both regular oscillations and random fluctuations, and the transition is caused by the emergence of new edge states when crossing the Landau levels. In the region of regular oscillation, the periods in the Fermi energy and in magnetic flux are related to the size of the device in a universal manner, regardless of the nature of the corresponding classical dynamics. The key to this universal scaling is the quantization of classically circulating edge orbits, which does not depend on the specific details of the geometrical shape of the dot. The details do appear in the fine-scale variations, where the random conductance fluctuations are typically smoother when the classical dynamics is chaotic.

ACKNOWLEDGMENTS

This work was supported by AFOSR under Grant No. FA9550-12-1-0095 and by ONR under Grant No. N00014-08-1-0627. L.H. was also supported by NSFC under Grant No. 11005053 and by the Fundamental Research Funds for the Central Universities.

[1] P. A. Lee and A. D. Stone, Phys. Rev. Lett. **55**, 1622 (1985); W. J. Skocpol, P. M. Mankiewich, R. E. Howard, L. D. Jackel, D. M. Tennant, and A. D. Stone, *ibid.* **56**, 2865 (1986); R. A. Jalabert, H. U. Baranger, and A. D. Stone, *ibid.* **65**, 2442 (1990); H. U. Baranger, R. A. Jalabert, and A. D. Stone, Chaos **3**, 665 (1993); Phys. Rev. Lett. **70**, 3876 (1993); Z. Qiao, J. Wang, Y. Wei, and H. Guo, *ibid.* **101**, 016804 (2008); K. M. D. Hals, A. K. Nguyen, X. Waintal, and A. Brataas, *ibid.* **105**, 207204 (2010); J. G. G. S. Ramos, D. Bazeia, M. S. Hussein, and C. H. Lewenkopf, *ibid.* **107**, 176807 (2011); R. Yang, L. Huang, Y.-C. Lai, and C. Grebogi, Phys. Rev. B **84**, 035426 (2011).

[2] R. Ketzmerick, Phys. Rev. B **54**, 10841 (1996); A. S. Sachrajda, R. Ketzmerick, C. Gould, Y. Feng, P. J. Kelly, A. Delage, and Z. Wasilewski, Phys. Rev. Lett. **80**, 1948 (1998); B. Huckestein, R. Ketzmerick, and C. H. Lewenkopf, *ibid.* **84**, 5504 (2000); L. Hufnagel, R. Ketzmerick, and M. Weiss, Europhys. Lett. **54**, 703 (2001); A. Bäcker, A. Manze, B. Huckestein, and R. Ketzmerick, Phys. Rev. E **66**, 016211 (2002); S. Löck, A. Backer, R. Ketzmerick, and P. Schlagheck, Phys. Rev. Lett. **104**, 114101 (2010).

[3] R. Blümel and U. Smilansky, Phys. Rev. Lett. **60**, 477 (1988); Y.-C. Lai, R. Blümel, E. Ott, and C. Grebogi, *ibid.* **68**, 3491 (1992).

[4] D. K. Ferry, R. Akis, and J. P. Bird, Phys. Rev. Lett. **93**, 026803 (2004).

[5] K. S. Novoselov, A. K. Geim, S. V. Morozov, D. Jiang, Y. Zhang, S. V. Dubonos, I. V. Grigorieva, and A. A. Firsov, Science **306**, 666 (2004); C. Berger, Z. Song, T. Li, X. Li, A. Y. Ogbazghi, R. Feng, Z. Dai, A. N. Marchenkov, E. H. Conrad, P. N. First, and W. A. de Heer, J. Phys. Chem. B **108**, 19912 (2004); K. S. Novoselov, A. K. Geim, S. V. Morozov, D. Jiang, M. I. Katsnelson, I. V. Grigorieva, S. V. Dubonos, and A. A. Firsov, Nature (London) **438**, 197 (2005); Y. Zhang, Y.-W. Tan, H. L. Stormer, and P. Kim, *ibid.* **438**, 201 (2005).

[6] C. W. J. Beenakker, Rev. Mod. Phys. **80**, 1337 (2008).

[7] A. H. Castro Neto, F. Guinea, N. M. R. Peres, K. S. Novoselov, and A. K. Geim, Rev. Mod. Phys. **81**, 109 (2009).

[8] S. Das Sarma, S. Adam, E. H. Hwang, and E. Rossi, Rev. Mod. Phys. **83**, 407 (2011).

[9] A. Rycerz, J. Tworzydlo, and C. W. J. Beenakker, Europhys. Lett. **79**, 57003 (2007).

[10] N. E. Staley, C. P. Puls, and Y. Liu, Phys. Rev. B **77**, 155429 (2008).

[11] R. Yang, L. Huang, Y.-C. Lai, and C. Grebogi, Europhys. Lett. **94**, 40004 (2011).

[12] K. S. Novoselov, Z. Jiang, Y. Zhang, S. V. Morozov, H. L. Stormer, U. Zeitler, J. C. Maan, G. S. Boebinger, P. Kim, and A. K. Geim, Science **315**, 1379 (2007).

[13] P. R. Wallace, Phys. Rev. **71**, 622 (1947); D. P. DiVincenzo and E. J. Mele, Phys. Rev. B **29**, 1685 (1984).

[14] J. W. McClure, Phys. Rev. **104**, 666 (1956); S. Xiong and A. D. Stone, Phys. Rev. Lett. **68**, 3757 (1992); D. L. Shepelyansky and A. D. Stone, *ibid.* **74**, 2098 (1995).

[15] J. P. Bird, K. Ishibashi, Y. Aoyagi, T. Sugano, R. Akis, D. K. Ferry, D. P. Pivin Jr., K. M. Connolly, R. P. Taylor, R. Newbury, D. M. Olatona, A. Micolich, R. Wirtz, Y. Ochiai, and Y. Okubo, Chaos Solitons Fractals **8**, 1299 (1997); D. K. Ferry, J. P. Bird, R. Akis, D. P. Pivin Jr., K. M. Connolly, K. Ishibashi, Y. Aoyagi, T. Sugano, and Y. Ochiai, Jpn. J. Appl. Phys. **36**, 3944 (1997); N. Holmbert, R. Akis, D. P. Pivin Jr., J. P. Bird, D. K. Ferry, Semicond. Sci. Technol. **13**, A21 (1999).

[16] Y. Ujiie, T. Morimoto, N. Aoki, D. K. Ferry, J. P. Bird, and Y. Ochiai, J. Phys.: Condens. Matter **21**, 382202 (2009).

[17] D. K. Ferry, L. Huang, R. Yang, Y.-C. Lai, and R. Akis, J. Phys. Conference Series **220**, 012015 (2010).

[18] S. Datta, *Electronic Transport in Mesoscopic Systems* (Cambridge University Press, Cambridge, England, 1995).

[19] S. V. Morozov, K. S. Novoselov, M. I. Katsnelson, F. Schedin, L. A. Ponomarenko, D. Jiang, and A. K. Geim, Phys. Rev. Lett. **97**, 016801 (2006); F. de Juan, A. Cortijo, and M. A. H. Vozmediano, Phys. Rev. B **76**, 165409 (2007); A. L. C. Pereira, C. H. Lewenkopf, and E. R. Mucciolo, *ibid.* **84**, 165406 (2011); Z. Wang and M. Devel, *ibid.* **83**, 125422 (2011); P. Partovi-Azar, N. Nafari, and M. R. Tabar, *ibid.* **83**, 165434 (2011); S. Costamagna, O. Hernandez, and A. Dobry, *ibid.* **81**, 115421 (2010); M. Gibertini, A. Tomadin, M. Polini, A. Fasolino, and M. I. Katsnelson, *ibid.* **81**, 125437 (2010).

[20] R. Landauer, Philos. Mag. **21**, 863 (1970).

[21] P. A. Lee and D. S. Fisher, Phys. Rev. Lett. **47**, 882 (1981).

[22] T. Ando, Phys. Rev. B **44**, 8017 (1991).

[23] T. C. Li and S.-P. Lu, Phys. Rev. B **77**, 085408 (2008).

[24] H.-J. Stöckmann, *Quantum Chaos: An Introduction* (Cambridge University Press, Cambridge, UK, 1999).

[25] H. A. Weidenmüller and G. E. Mitchell, Rev. Mod. Phys. **81**, 539 (2009).

[26] M. C. Gutzwiller, J. Mathematical Physics **12**, 343 (1970).

[27] For semiconductor 2DEG systems, we have $E = \hbar^2 k^2/2m^*$ and $D = k\ell_B^2$. The scaling relation becomes $D = \sqrt{2m^* E}/eB$, where m^* is the effective mass of the electron.

[28] D. A. Bahamon, A. L. C. Pereira, and P. A. Schulz, Phys. Rev. B **79**, 125414 (2009).

[29] L. Huang, Y. C. Lai, D. K. Ferry, S. M. Goodnick, and R. Akis, Phys. Rev. Lett. **103**, 054101 (2009).

[30] L. Huang, Y. C. Lai, and C. Grebogi, Chaos **21**, 013102 (2011).

[31] U. Fano, Phys. Rev. **124**, 1866 (1961).

[32] R. Yang, L. Huang, Y.-C. Lai, and L. M. Pecora, Appl. Phys. Lett. **100**, 093105 (2012).